A plasma photonic crystal bandgap device

Cite as: Appl. Phys. Lett. **108**, 161101 (2016); https://doi.org/10.1063/1.4946805
Submitted: 02 December 2015 . Accepted: 07 March 2016 . Published Online: 18 April 2016

B. Wang, and M. A. Cappelli

A plasma photonic crystal bandgap device

B. Wang and M. A. Cappelli
Stanford Plasma Physics Laboratory, Department of Mechanical Engineering, Stanford University, Stanford, California 94305, USA

(Received 2 December 2015; accepted 7 March 2016; published online 18 April 2016)

A fully tunable plasma photonic crystal is used to control the propagation of free space electromagnetic waves in the S to X bands of the microwave spectrum. An array of discharge plasma tubes forms a simple square crystal structure with the individual plasma dielectric constant tuned through variation in the plasma density. We show, through simulations and experiments, that transverse electric mode bandgaps exist, arising from the positive and negative dielectric constant regimes of the plasma, and that the respective bandgap frequencies can be shifted through changing the dielectric constant by varying discharge current density. *Published by AIP Publishing.*
[http://dx.doi.org/10.1063/1.4946805]

The first demonstrations of photonic crystal (PC) devices were carried out in the Ku band of the electromagnetic (EM) spectrum using an array of alumina lattice elements.[1] Since then, PC devices that operate into the terahertz (THz)[2] and optical[3] regimes have been demonstrated. The photonic bandgaps of the first devices were not actively tunable. Over the past decade, methods to achieving bandgap tunability have included mechanical,[2] thermal,[4] and opto-fluidic strategies.[5]

The use of gaseous plasma elements as PCs was first demonstrated by Sakai *et al.*[6] All-plasma arrays,[6,7] as well as single plasma elements in solid structure metallic[8] and dielectric[9] arrays, provide a means of achieving active bandgap and defect state pass-band tunability at relatively high rates by the ability to vary plasma density. These rates, limited by the ionization or recombination times of the plasma, can be significantly higher than those limited by mechanical, thermal, or fluidic time scales. Experimentally realizable gaseous plasma devices have operating frequencies that are controlled by the plasma frequency of the discharges. Plasma-based bandgap devices have been explored through modeling and simulations,[10] and through experimental testing.[6,11] A unique feature of full plasma photonic crystals with square lattice configurations is the preference for transverse electric (TE) propagation bandgap modes due to the excitation of surface plasma waves.[6,7]

As in their solid structure counterparts, an all-plasma photonic crystal will have characteristic bandgaps that are a result of successive Bragg scattering between the plasma interfaces. Like metallic structures, the dielectric constant can range from strongly negative to positive values of less than unity (passing through zero), depending on the EM wave frequency and electron density. A significant challenge in the construction of a device based on an all-plasma array photonic crystal is the control of plasma elements that are individually tunable and switchable to provide rapid reconfigurability that exploits this range in dielectric constant—a feature not afforded by traditional dielectrics. Another challenge is that the plasma elements must have a low collisionality in order to reduce signal attenuation that results in suboptimal performance. Our previous work on integrating a single plasma element into an alumina photonic crystal device demonstrated active tunability using the plasma element as the tuning source.[12] A natural extension of the tunable device is a plasma photonic crystal that is completely formed from plasma elements.

In this letter, we present the EM wave transmission characteristics of an all-plasma photonic crystal that operates in the S through X bands of the microwave region of the EM spectrum. Our focus is on simulating and experimentally demonstrating the existence of bandgaps attributed to both the positive and negative dielectric constants of the plasma.

Figure 1 presents a schematic diagram of the device studied. The basic structure is that of a two-dimensional (2-D) periodic array of circular plasma elements arranged in a square lattice. In the device simulated and tested experimentally, the plasma elements consist of individually controllable alternating-current (AC) discharge tubes. The discharge tubes were arranged with a lattice constant of 38.1 mm, forming a 7 by 7 square array. A 15 mm diameter quartz ($\varepsilon = 3.8$) tube with an inner wall thickness of 1 mm and length of 290 mm, filled with argon to a pressure of 250 Pa and added mercury, serves as the discharge plasma. The discharge temperature was estimated to be around 330 K,[13] giving a mercury vapor partial pressure of about 3.5 Pa.[14] Each discharge was driven individually by an AC ballast with a peak to peak voltage of 160 V. The voltage waveform of each discharge was triangular in shape resulting in a root-mean-square (RMS) voltage of

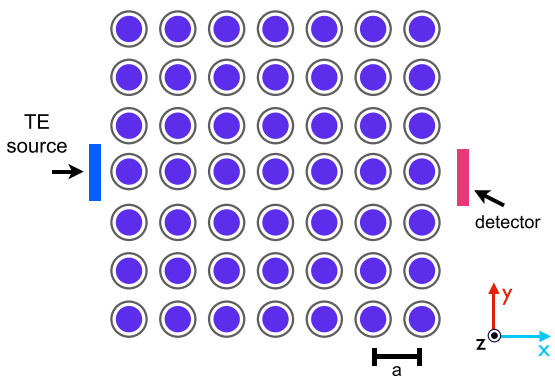

FIG. 1. (a) A 7 by 7 plasma photonic crystal array with lattice constant a = 38.1 mm.

$V_{RMS} = 80/\sqrt{3}$ V. The ballast had a variable peak current (also close to triangular in wave form) to control the discharge parameters, ranging from 24.8 mA to 111.1 mA, with a ballast frequency that decreased linearly from 55.0 kHz to 37.0 kHz for increasing peak current in the range from 24.8 mA to 51.2 mA, and a ballast frequency in the range of 32.2 kHz–33.8 kHz for peak discharge currents from 54.4 mA to 111.2 mA.

The variable discharge current controls the plasma density which determines the location of the zero-point in the real part of the dielectric constant (epsilon-zero frequency), i.e., the frequency corresponding to the plasma frequency of the discharge elements. Source frequencies spanning this epsilon-zero condition allow us to map the bandgaps associated with both epsilon positive and epsilon negative regimes, and the associated broadening and shifting of these bandgaps that arise when the plasma density is varied.

When the frequency is less than (or greater than) the plasma frequency, the plasma dielectric constant is negative (or positive) but reverts to the dielectric constant of air when the plasma is turned off. For the designed device, we utilize both the positive and negative dielectric constant values to form bandgaps. With all plasma elements active, the photonic crystal structure acts as a TE mode band gap device. Varying the plasma density allows for the bandgap to shift in frequency and change in width.

To anticipate the approximate locations of where the bandgaps associated with the negative and positive epsilon regimes of the plasma will appear, calculations were first carried out using the High Frequency Electromagnetic Field Simulator (formally known as the High Frequency Structural Simulator) ANSYS HFSS 16, simulating the transmission properties of a 7× infinite array of dielectric rods. The rods were assigned to have a diameter and lattice constant equal to that of the plasma array, and dielectric constants equal to that of a plasma density of $n_e = 5.8 \times 10^{11}\,\mathrm{cm}^{-3}$, a value that is expected in these discharge tubes at a current of 34.4 mA.[12] For these simulations, an assigned dielectric constant of −1.75 corresponds to that of this plasma at 4.0 GHz, while an assigned dielectric constant of +0.20 corresponds to that of this plasma at 7.6 GHz. Figure 2 shows the HFSS simulated transmission spectra $|S_{21}|$ for the photonic crystal. In the negative epsilon regime, there is a bandgap between 3 GHz and 4.5 GHz with an attenuation of approximately 15 dB. The positive epsilon regime has a bandgap between 7.5 and 8.5 GHz, with a much smaller rejection attenuation (less than 3 dB) as a result of the lower dielectric constant. The two permittivity regimes allow the crystal to operate as either a device with negative permittivity rods in air or a dielectric air slab with positive but lower permittivity plasma holes. The negative permittivity bandgap in this TE excitation is a consequence of the gap between the flat bands associated with surface plasma propagation and the first Bloch state at the X point below the plasma frequency.[15]

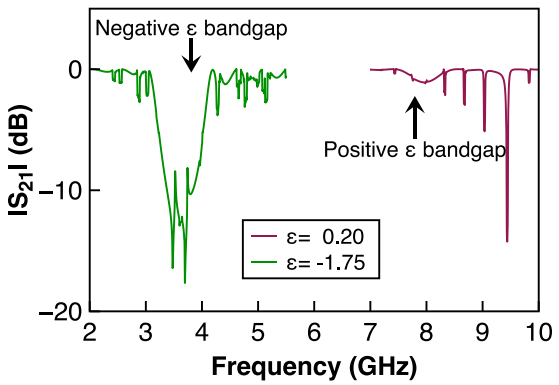

FIG. 2. Simulated transmission ($|S_{21}|$) for a 7 by infinite array photonic crystal with circular elements having positive ($\varepsilon = 0.20$) and negative ($\varepsilon = -1.75$) permittivities.

Simulations of the plasma photonic crystal with various plasma densities were completed using HFSS. The two-dimensional simulations consider the case of an infinite plasma column height and an infinite number of elements in the y-direction through setting appropriate periodic boundary conditions. For TE polarization, perfectly magnetic conductor (PMC) boundaries assumed at the top and bottom interfaces of a single array of 7 plasma columns simulate the case of an infinite height. A perfectly electric conductor (PEC) boundary condition placed a half lattice constant away from the center axis of the rods mirror the rods in the y-axis direction.[7,16] The boundary conditions simulate a 7 (x-direction) by infinite (y-direction) by infinite (z-direction) array of rods. Both the plasma and the quartz envelope were included in the simulations.

The HFSS simulations require specifying the plasma density distribution within the discharge tube. The plasma experiences radial diffusion due to wall recombination with a radial electron density distribution that is expected to be near parabolic in shape. For our simulations, we simplified the plasma distribution by assuming that the plasma electrons are distributed uniformly over a diameter that is $1/\sqrt{2}$ times the inner discharge tube diameter such that the plasma diameter is 9.2 mm, to form a region of higher electron density that is twice that if the electrons were distributed uniformly over the entire inner tube diameter of d = 13 mm. We define the plasma density over this reduced region of uniform plasma density (diameter of 9.2 mm) as n_e.

The plasma is assumed to have a dielectric constant that is described by the Drude model

$$\varepsilon_p(\omega) = 1 - \frac{\omega_p^2}{\omega^2 - i\gamma\omega}. \tag{1}$$

Here, γ is the total momentum transfer collision frequency of the plasma electrons. The plasma frequency is equal to

$$\omega_p = \sqrt{\frac{n_e e^2}{m_e \varepsilon_0}}, \tag{2}$$

where e is the electron charge, m_e is the electron mass, and ε_o is the free space permittivity. The plasma density and thus the plasma frequency and dielectric constant are tunable parameters controlled by varying the discharge current. The dielectric constant and its variation with frequency and plasma density is shown in Fig. 3. We use the electron energy distribution function solver, BOLSIG,[17] which provides a solution to the Boltzmann equation for the electrons and associated transport properties, to estimate the total

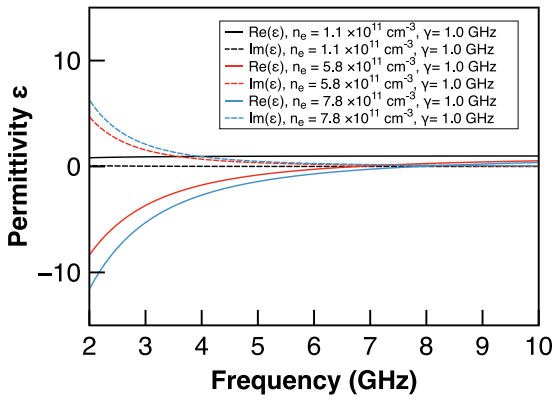

FIG. 3. Real and imaginary components of the plasma relative permittivity for various plasma densities.

electron momentum transfer collision frequency. For the range of discharge conditions used here, $\gamma \approx 1.0$ GHz.

For the experiment, a pair of microwave broadband (2 GHz–18 GHz) horns are used as the source and detector antennas set to the TE polarization, each connected to an HP 8722D Vector Network Analyzer to measure the transmission coefficient. The TE source polarization is defined as having the electric field vector oriented in the y axis, such that it is perpendicular to the plasma discharge element. The measured transmission was recorded with an integration time of 5 ms per frequency point in the scan. Figure 4 shows the experimental setup with the plasma photonic crystal array and microwave horns. The individual ballasts are not in phase with one another; however, simulations on similar discharges have shown that the plasma density is essentially unchanging over each current cycle and does not respond to the high frequency (40 kHz) current waveforms.[18]

Figure 5 shows the experimental transmission spectra $|S_{21}|$ for three cases of the discharge current. The ratio of the dielectric constant of the plasma to that of the surrounding air ($\varepsilon_p/\varepsilon_{air}$) effects the shape and strength of the bandgap.[19] Three different plasma parameters are presented to illustrate the bandgap tunability. The band gap opens for plasma densities $n_e > 5.8 \times 10^{11}\,\mathrm{cm}^{-3}$. As predicted by the calculations shown in Fig. 2, we see the development of two bandgaps, centered at about 4 GHz and 8 GHz, at the higher plasma densities. The strength of the bandgaps increases strongly and shifts to higher frequencies with increased plasma density. This shift is due to the increased plasma frequency which defines the zero-epsilon condition.

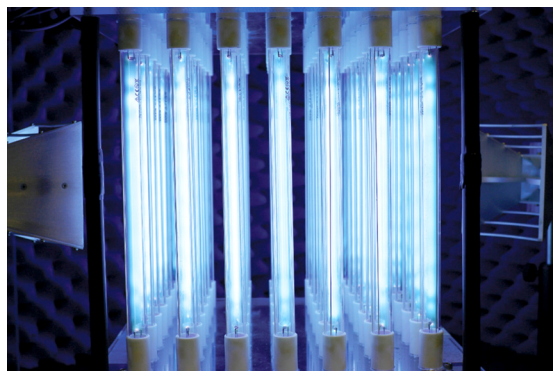

FIG. 4. Experimental setup with plasma photonic crystal array and measurement setup. An acrylic base structure is used to support the device.

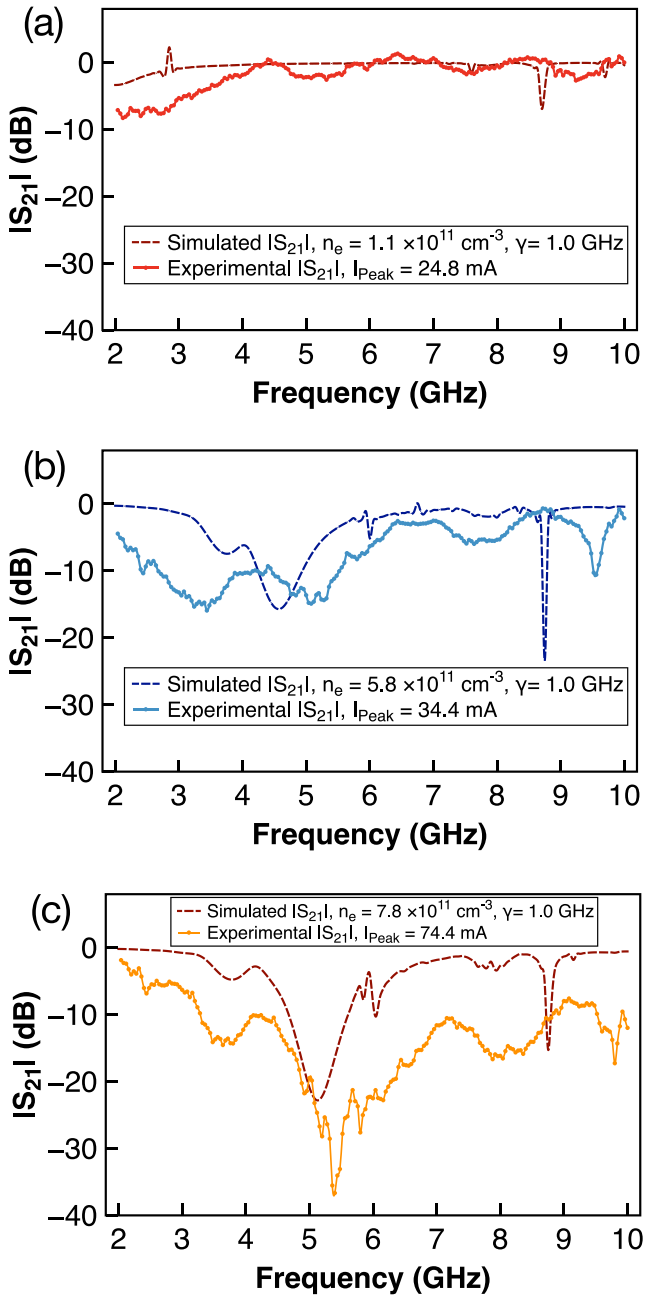

FIG. 5. Simulated transmission spectra for the plasma photonic crystal device vs. experimental transmission spectra for various peak plasma discharge currents and plasma densities. The primary and secondary bandgaps are seen in the transmission spectra in (b) and (c).

Also shown in Fig. 5 are the transmission spectra predicted by the simulations. The values for the plasma density used in the simulations were estimated from our previous studies.[12] At a discharge current of 24.8 mA, the plasma dielectric constant is very close to unity and we predict free transmission from 4 GHz to 10 GHz, in good agreement with experiments. The structure that develops in the region below about 3 GHz occurs where the dielectric constant of the plasma falls below the plasma frequency. In this region, the Im(ε) is significant, and leads to an attenuation of the signal to −7 dB. The experiments also suggest some attenuation in this region at these low plasma densities. At the highest

discharge current investigated (74.4 mA), the simulations predict a strong bandgap between 3 GHz and 6 GHz due to the negative epsilon plasma contribution, and a weaker bandgap between 7 GHz and 8 GHz. The simulations have a sharp attenuation drop around 9 GHz due to the periodic quartz envelopes, which was observed when the plasma elements were removed in the simulations. Experimentally, the plasma has an interface with the quartz that was not modeled in the simulations, explaining the increased scattering and reflection at higher plasma densities around 9 GHz. The simulations are in good agreement with the experiments, although shifted slightly towards lower frequencies, suggesting perhaps that the plasma densities used in the simulations are slightly higher than those in the discharge tube at these current densities. Similar agreement is seen for the intermediate case of 34.4 mA in discharge current. The experimental results here have expected signal leakage and scattering in the z axis due to the three dimensional structure of the device, which corresponds to the attenuation found in the passbands of the photonic crystal.

The results presented here confirm that all-plasma photonic crystals can develop strong bandgaps, particularly at high plasma density conditions. The lower frequency regime at conditions below cut-off affords the most favorable conditions, where a relatively strong bandgap develops that is tunable with discharge current. In this regime, the device is characterized as an array of negative permittivity plasma rods in air, with TE modes being preferred as a consequence of surface plasmon effects.[15] The weak bandgap that forms at conditions above the cut-off frequency is due to positive epsilon contribution from the plasma, with the air acting as a high dielectric constant slab with plasma holes acting as the material of lower dielectric constant. This is a unique mode of operation that allows for TE bandgap formation in frequencies above the critical plasma frequency. The device described here extends our previous work that demonstrates the integration of a plasma element into a dielectric (alumina) photonic crystal array. The characterization and design of this all-plasma photonic crystal structure will provide the groundwork for other operational modes that are a result of the switchability of the plasma elements, as well as an increased understanding of the interactions between electromagnetic waves and plasma based photonic devices. Future experiments will investigate reconfigurable waveguiding, bends, and cavity modes.

This work was supported in part by a Multidisciplinary University Research Initiative from the Air Force Office of Scientific Research. B.W. was also supported in part by a National Defense Science and Engineering Graduate Fellowship.

[1]E. Yablonovitch, "Photonic band-gap structures," J. Opt. Soc. Am. B **10**, 283 (1993).
[2]J. Kitagawa, M. Kodama, S. Koya, Y. Nishifuji, D. Armand, and Y. Kadoya, "THz wave propagation in two-dimensional metallic photonic crystal with mechanically tunable photonic-bands," Opt. Express **20**, 17271–17280 (2012).
[3]I. El-Kady, M. M. Sigalas, R. Biswas, K. M. Ho, and C. M. Soukoulis, "Metallic photonic crystals at optical wavelengths," Phys. Rev. B **62**, 15299–15302 (2000).
[4]H. M. H. Chong and R. M. De La Rue, "Tuning of photonic crystal waveguide microcavity by thermooptic effect," IEEE Photonics Technol. Lett. **16**, 1528–1530 (2004).
[5]D. Yang, H. Tian, and Y. Ji, "Nanoscale photonic crystal sensor arrays on monolithic substrates using side-coupled resonant cavity arrays," Opt. Express **19**, 20023 (2011).
[6]O. Sakai, T. Sakaguchi, Y. Ito, and K. Tachibana, "Interaction and control of millimetre-waves with microplasma arrays," Plasma Phys. Controlled Fusion **47**, B617–B627 (2005).
[7]L. Qi, C. Li, G. Fang, and X. Gao, "The absorbing properties of two-dimensional plasma photonic crystals," Plasma Sci. Technol. **17**, 4–9 (2015).
[8]J. Lo, J. Sokoloff, T. Callegari, and J. P. Boeuf, "Reconfigurable electromagnetic band gap device using plasma as a localized tunable defect," Appl. Phys. Lett. **96**, 251501 (2010).
[9]S. Varault, B. Gabard, J. Sokoloff, and S. Bolioli, "Plasma-based localized defect for switchable coupling applications," Appl. Phys. Lett. **98**, 134103 (2011).
[10]Q. Li-Mei, Y. Zi-Qiang, L. Feng, G. Xi, and L. Da-Zhi, "Dispersion characteristics of two-dimensional unmagnetized dielectric plasma photonic crystal," Chin. Phys. B **19**, 034210 (2010).
[11]O. Sakai, T. Sakaguchi, and K. Tachibana, "Photonic bands in two-dimensional microplasma arrays. I. Theoretical derivation of band structures of electromagnetic waves," J. Appl. Phys. **101**, 073304 (2007).
[12]B. Wang and M. A. Cappelli, "A tunable microwave plasma photonic crystal filter," Appl. Phys. Lett. **107**, 171107 (2015).
[13]C. Kenty, M. A. Easley, and B. T. Barnes, "Gas temperatures and elastic losses in low pressure mercury-argon discharges," J. Appl. Phys. **22**, 1006 (1951).
[14]M. L. Huber, A. Laesecke, and D. G. Friend, "The vapor pressure of mercury," NIST Interagency/Internal Report No. NISTIR 6643, 2006.
[15]T. Ito and K. Sakoda, "Photonic bands of metallic systems. II. Features of surface plasmon polaritons," Phys. Rev. B **64**, 045117 (2001).
[16]J. D. Shumpert, W. J. Chappell, and L. P. B. Katehi, "Parallel-plate mode reduction in conductor-backed slots using electromagnetic bandgap substrates," IEEE Trans. Microwave Theory Tech. **47**, 2099–2104 (1999).
[17]G. J. M. Hagelaar and L. C. Pitchford, "Solving the Boltzmann equation to obtain electron transport coefficients and rate coefficients for fluid models," Plasma Sources Sci. Technol. **14**, 722–733 (2005).
[18]K. Loo, D. Stone, and R. Tozer, "Modeling the electrical behavior of fluorescent lamps on the basis of a self-consistent collisional-radiative model," in *Industry Applications Conference* (2004), Vol. 3, pp. 1646–1654.
[19]J. D. Joannopoulos, S. G. Johnson, J. N. Winn, and R. D. Meade, *Photonic Crystals Molding the Flow of Light*, 2nd ed. (Princeton University Press, Princeton, New Jersey, 2008).